Inorganic Chemistry

pubs.acs.org/IC Article

Synthesis of $[Ni_{23}Se_{12}X_3(PEt_3)_{10}]$ (X = Br, I) via Post-synthetic Modification

Phoebe R. Hertler, Alexander J. Touchton, Guang Wu, Tieyan Chang, Ying-Pin Chen, Yu-Sheng Chen, and Trevor W. Hayton*

Cite This: *Inorg. Chem.* 2025, 64, 2926−2935 Read Online

ACCESS | Metrics & More | Article Recommendations | Supporting Information

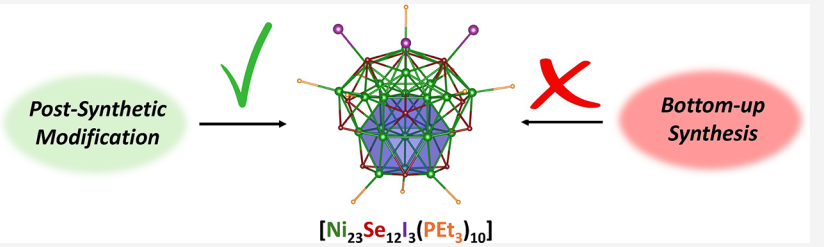

ABSTRACT: Treatment of $[Ni_{23}Se_{12}Cl_3(PEt_3)_{10}]$ (**1-Cl**) with excess Me_3SiX (X = Br, I) results in formation of $[Ni_{23}Se_{12}X_3(PEt_3)_{10}]$ (X = Br, **1-Br**; X = I, **1-I**) in good yields. **1-Br** and **1-I** are exceptionally rare examples of atomically precise nickel nanoclusters (APNCs). Both **1-Br** and **1-I** were characterized by X-ray crystallography, NMR spectroscopy, and ESI-mass spectrometry. Both clusters feature a compact $[Ni_{13}]^{7+}$ kernel capped by a $[Ni_{10}(\mu\text{-Se})_9X_3]^-$ shell. Cluster **1-Br** could also be isolated cleanly using a bottom-up synthetic approach, via reaction of $[Ni(1,5\text{-cod})_2]$ and PEt_3 with $SePEt_3$ and $[NiBr_2(PEt_3)_2]$. Under these conditions, it could be isolated in 43% yield. In contrast, reaction of $[Ni(1,5\text{-cod})_2]$ and PEt_3 with $SePEt_3$ and $[NiI_2(PEt_3)_2]$ results in formation of $[Ni_3(\mu_3\text{-Se})_2I_2(PEt_3)_4]$ (**2-I**) as the only isolable product. These results highlight the challenges inherent in the bottom-up synthesis of Ni nanoclusters, and demonstrate the value of postsynthetic modification in the synthesis of 3d metal APNCs.

INTRODUCTION

Transition metal APNCs are of interest for a variety of applications, spanning catalysis, electronics, magnetic data storage, and quantum computing.[1−7] Clusters featuring Fe, Co, and Ni are particularly appealing for magnetic applications because these elements are ferromagnetic in bulk form. However, little headway has been made on isolating nanoclusters of these elements.[8] Indeed, a search of the Cambridge Crystallographic Database reveals only four reported Fe nanoclusters,[9] four reported Co nanoclusters,[10−12] and ten reported Ni nanoclusters;[13−22] defined here as a cluster that contains at least one central metal atom coordinated to at least eight other metal atoms and no nonmetal atoms. In contrast, there are approximately 190 and 370 APNC nanoclusters structures reported for Ag and Au, respectively.[23] Their paucity is due to a number of factors, including their high air sensitivity, paramagnetism, unfavorable redox properties, relatively low M−M bond enthalpies, and lack of suitable starting materials.[8,24−28]

Given the challenge of generating APNCs of Fe, Co, and Ni via the traditional bottom-up approaches, the use of postsynthetic modification could be a valuable strategy for making new nanoclusters of these elements. In fact, postsynthetic ligand exchange is emerging as an important tool in nanocluster synthesis.[29−34] For example, reaction of $[IrAu_{12}(dppe)_5Cl_2]^+$ with KX (X = Br, I) yielded $[IrAu_{12}(dppe)_5X_2]^+$ (dppe = 1,2-bis(diphenylphosphino)-ethane; X = Br, I) via halide exchange. The modified clusters exhibited improved photoredox properties, highlighting the utility of post synthetic modification in tuning APNC properties.[35] Similarly, reaction of $[Au_{11}(dppf)_4Cl_2]Cl$ with KX (X = Br, I, SCN) yielded the isostructural APNCs, $[Au_{11}(dppf)_4X_2]X$ (dppf = 1,1′-bis(diphenylphosphino)-ferrocene).[36] Of greater relevance to the current work, reaction of the rare Fe APNC, $[(Tp^*WS_3)_4Fe_{13}]$, with Me_3SiN_3 or PhN_3 leads to formation of the oxidized clusters, $[(Tp^*WS_3)_4Fe_{13}(\mu_3\text{-N})_4]$ and $[(Tp^*WS_3)_4Fe_{13}(\mu_3\text{-NPh})_3]$, respectively, demonstrating the ability to tune oxidation state for potential magnetic applications.[9]

In each of the above-mentioned cases, the APNC nuclearity and core structure did not change. In contrast, many attempts at postsynthetic modification lead to large, and potentially

Received: November 27, 2024
Revised: January 10, 2025
Accepted: January 24, 2025
Published: February 3, 2025

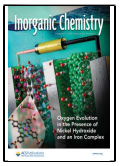

https://doi.org/10.1021/acs.inorgchem.4c05088
Inorg. Chem. 2025, 64, 2926−2935

Scheme 1. Synthesis of $[Ni_{23}Se_{12}Cl_3(PEt_3)_{10}]$ (1-Cl) and $[Ni_3(\mu_3\text{-}Se)_2Cl_2(PEt_3)_4]$ (2-Cl)

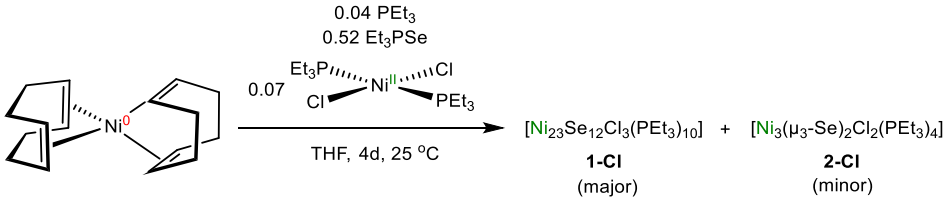

Scheme 2. Syntheses of 1-Br and 1-I via Post-synthetic Modification and Bottom-Up Synthesis

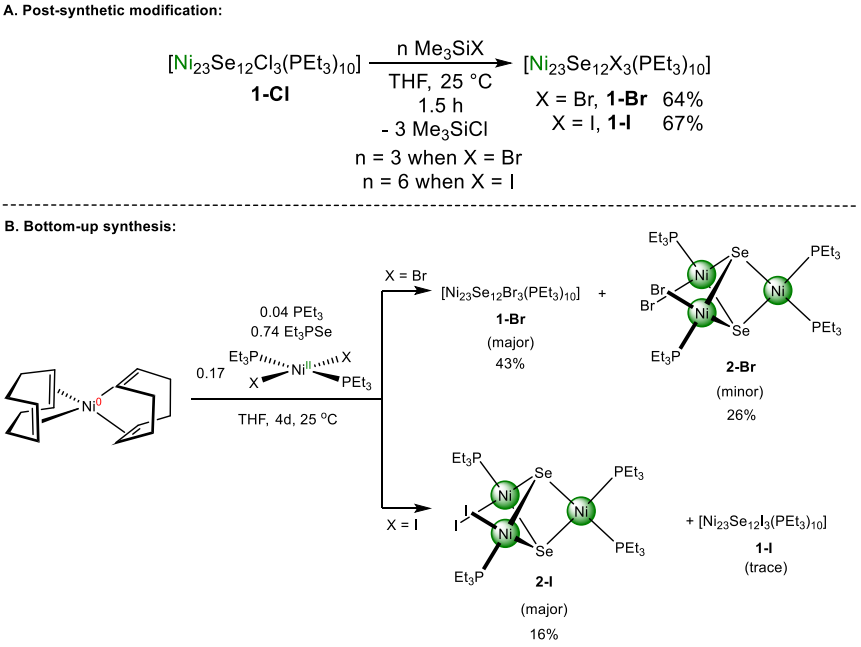

undesirable, structural and/or nuclearity changes.[30,34,37−42] For example, addition of Ph_2phen to $[Cu_{25}H_{22}(PPh_3)_{12}]Cl$ results in isolation of a Cu_{29} cluster, $[Cu_{29}Cl_4H_{22}(Ph_2phen)_{12}]Cl$ (Ph_2phen = 4,7-diphenyl-1,10-phenanthroline) via sacrificial disassembly of the Cu_{25} starting material.[43] Similarly, reaction of $[Ag_{32}S_3(CC^tBu)_{23}]^{3+}$ with 3-bromophenylacetylene results in isolation of the larger Ag_{45} APNC, $[Ag_{45}S_6(CCC_6H_4\text{-}3\text{-}Br)_{32}]^+$,[44] whereas reaction of $[Au_{23}(S\text{-}cyclo\text{-}C_6H_{11})_{16}]^-$ with 1-adamantanethiol leads to formation of the smaller Au_{16} APNC, $[Au_{16}(S\text{-}1\text{-}Ad)_{12}]$.[42] In these cases, the changes in nuclearity can be ascribed to the different donor abilities, denticities, and steric properties of the incoming ligand.[42−44]

Recently, we reported the synthesis of a rare Ni-containing nanocluster, $[Ni_{23}Se_{12}Cl_3(PEt_3)_{10}]$ (**1-Cl**).[14] This cluster was synthesized by treatment of $[Ni(1,5\text{-}cod)_2]$ with PEt_3, $SePEt_3$, and $[NiCl_2(PEt_3)_2]$ (Scheme 1). The reaction to form **1-Cl** is highly reproducible and the crystallization is well behaved, allowing isolation of the cluster in good yields as analytically pure material. Also formed in the reaction, as a minor product, is the Ni_3 cluster, $[Ni_3(\mu_3\text{-}Se)_2Cl_2(PEt_3)_4]$ (**2-Cl**), which was also structurally characterized. Cluster **2-Cl** is easily separated from **1-Cl**. Interestingly, **1-Cl** was first reported in 1992, but it was originally formulated as $[Ni_{23}Se_{12}(PEt_3)_{13}]$ on the basis of low quality X-ray diffraction data.[17]

Given the relatively high yield of **1-Cl**, coupled with its ease of preparation, and the presence of potentially exchangeable chloride ligands, we hypothesize that it would be a good candidate for postsynthetic modification. Herein, we describe the synthesis of $[Ni_{23}Se_{12}X_3(PEt_3)_{10}]$ (X = Br, I), which were formed by postsynthetic halide metathesis. The bromide analogue was also synthesized via a bottom-up approach, whereas the iodide analog could not be isolated in this manner, conclusively demonstrating that postsynthetic modification is a valuable strategy for the synthesis of new 3d metal nanoclusters.

RESULTS AND DISCUSSION

Synthesis and Characterization of $[Ni_{23}Se_{12}X_3(PEt_3)_{10}]$ (X = Br, I). We hypothesized that we could access clusters **1-Br** and **1-I** via halide metathesis from **1-Cl**, using Me_3SiX (X = Br, I) as the halide source. While halide metathesis with Me_3SiX is not well established in nanocluster synthesis, this protocol is well-known in organometallic chemistry.[45,46] Previous examples of APNC halide exchange used alkali metal salts,[35,36] which are not as easy to remove as the volatile silicon reagent. Thus, treatment of **1-Cl** with 3 equiv of Me_3SiBr in tetrahydrofuran (THF) at room temperature results in formation of $[Ni_{23}Se_{12}Br_3(PEt_3)_{10}]$ (**1-Br**), which can be isolated in 64% yield upon workup (Scheme 2A). Similarly, reaction of **1-Cl** with 6 equiv of Me_3SiI in THF results in formation of $[Ni_{23}Se_{12}I_3(PEt_3)_{10}]$ (**1-I**), which can be isolated in 67% after workup. Cluster **1-I** could also be made by reaction of **1-Cl** with excess NaI, but the yield was not as good (see Supporting Information for more details). Interestingly, reaction of **1-Br** with Me_3SiI did not result in formation of **1-I**. Instead, we observe the formation of $[Ni_{23}Se_{12}Br_{3-n}I_n(PEt_3)_{10}]$ (n = 1, 2) as the major products, along with the presence of unreacted starting material, according to ESI-MS (Figure S40),

https://doi.org/10.1021/acs.inorgchem.4c05088
Inorg. Chem. 2025, 64, 2926−2935

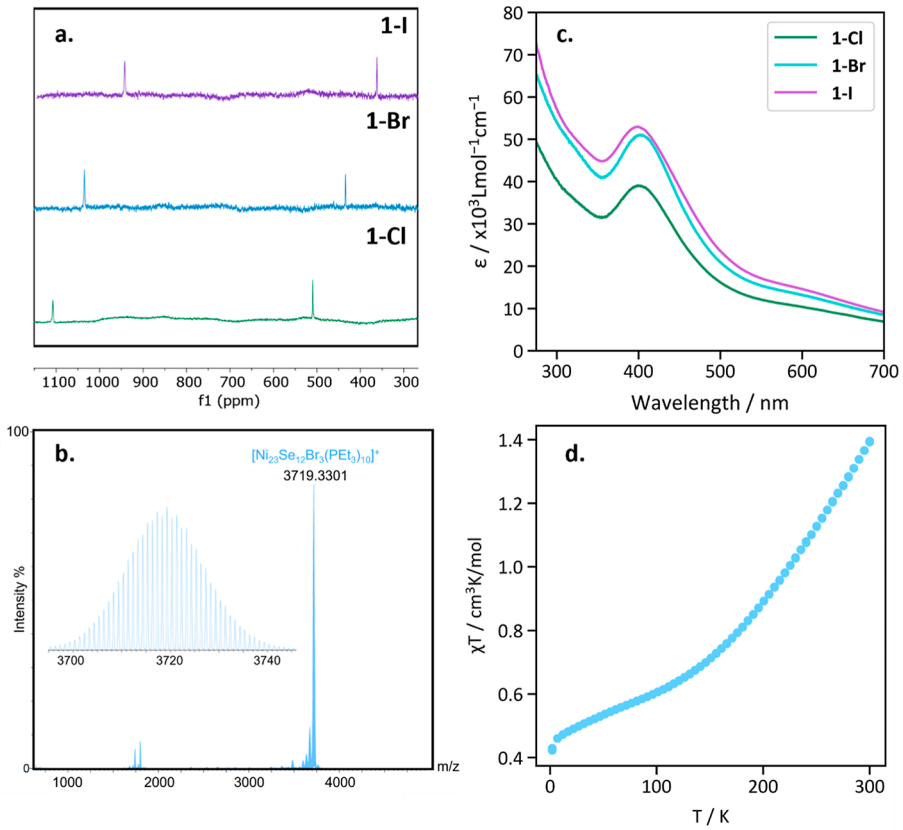

Figure 1. (a) Room temperature $^{31}P\{^{1}H\}$ NMR spectra of **1-Cl**, **1-Br** and **1-I** recorded in C_6D_6. $^{31}P\{^{1}H\}$ NMR data for **1-Cl** taken from ref 14. (b) ESI-MS of $[\mathbf{1\text{-}Br}]^+$, recorded in THF (3.00 kV capillary voltage, positive ion mode). (c) UV−vis absorption spectra of **1-Cl**, **1-Br**, and **1-I** in THF at 298 K. d. Variable-temperature magnetic susceptibility (χT) data for **1-Br** collected under an applied magnetic field of H = 1000 Oe (0.1 T) from T = 2 to T = 300 K.

presumably due to the lack of strong thermodynamic driving force. Finally, reaction of **1-Cl** with 3 equiv of Me_3SiN_3 did not result in any reaction after 24 h, whereas reaction of **1-Cl** with 3 equiv of Me_3SiOTf resulted in cluster decomposition.

Cluster **1-Br** is soluble in THF, sparingly soluble in benzene and toluene, and insoluble in diethyl ether, pentane, hexanes, and acetonitrile. Cluster **1-I** is soluble in THF, toluene, and benzene, sparingly soluble in diethyl ether, and insoluble in pentane and hexanes. The ^{1}H NMR spectrum of **1-Br** in benzene-d_6 (25 °C) features resonances at 7.11, 1.83, and 1.15 ppm, in a 9:54:27 ratio, respectively. These resonances are assignable to the three unique methyl environments of the 10 PEt_3 ligands, and are consistent with the C_3 symmetry observed in the solid state (see below for more discussion). The ^{1}H NMR spectrum also features a resonance at 43.45 ppm, which corresponds to the methylene environment of the apical PEt_3 ligand, resonances at 5.51 and 5.36 ppm, which correspond to the diastereotopic methylene environments of the six equatorial PEt_3 ligands, and a multiplet at 3.38 ppm, which corresponds to the remaining methylene environment. The $^{31}P\{^{1}H\}$ spectrum of the same benzene-d_6 solution features resonances at 434 and 1035 ppm in a 3:6 ratio (Figure 1a). These resonances account for the three PEt_3 ligands at the base of the cluster, and the six PEt_3 ligands bound to the equatorial belt. The resonance for the apical PEt_3 was not observed, presumably because of paramagnetic broadening. The ^{1}H and $^{31}P\{^{1}H\}$ NMR spectral properties of **1-I** are similar, suggesting a comparable structure. In particular, its $^{31}P\{^{1}H\}$ NMR spectrum consists of two extremely downfield shifted resonances at 362 and 942 ppm in a 3:6 ratio (Figure 1a).

The ESI-MS spectra of isolated **1-Br** and **1-I** confirm the new formulations and successful halide exchange. The spectrum of **1-Br** in THF (3.00 kV capillary voltage, positive ion mode) displays a major peak at 3719.3301 m/z assignable to $[Ni_{23}Se_{12}Br_3(PEt_3)_{10}]^+$ ($[\mathbf{1\text{-}Br}]^+$, calcd 3719.1492 m/z) (Figure 1b). Excellent agreement is observed between the experimental and simulated isotope patterns for this ion (Figure S32), providing further support for its formulation. We also observe a minor peak at 3675.3684 m/z, which is assignable to $[Ni_{23}Se_{12}Br_2Cl(PEt_3)_{10}]^+$ ($[\mathbf{1\text{-}Br}$ − Br + Cl$]^+$, calcd 3673.1997 m/z). We suggest that formation of $[\mathbf{1\text{-}Br}$ − Br + Cl$]^+$ is due to halide exchange with adventitious chloride in the ESI-MS injection line, and not due to partial halide exchange during the reaction. Adventitious chloride incorporation into APNCs has been observed previously by several different groups.[47−49] We also observed adventitious halide exchange in the ESI-MS of **1-Cl**.[14] The ESI-MS of **1-I** in THF (3.00 kV capillary voltage, positive ion mode) displays a major peak at 3859.6699 m/z, assignable to $[Ni_{23}Se_{12}I_3(PEt_3)_{10}]^+$ ($[\mathbf{1\text{-}I}]^+$, calcd 3859.1121 m/z). As with $[\mathbf{1\text{-}Br}]^+$, we observe excellent agreement between experimental and simulated isotope patterns for $[\mathbf{1\text{-}I}]^+$ (Figure S39). We also observe smaller peaks at 3813.2541 and 3766.6753 m/z, which are assignable to $[Ni_{23}Se_{12}I_2Br(PEt_3)_{10}]^+$ ($[\mathbf{1\text{-}I}$ − I + Br$]^+$, calcd 3813.1443 m/z) and $[Ni_{23}Se_{12}I_2Cl(PEt_3)_{10}]^+$ ($[\mathbf{1\text{-}I}$ − I + Cl$]^+$, calcd 3766.1980 m/z), respectively. We hypothesize that their

https://doi.org/10.1021/acs.inorgchem.4c05088
Inorg. Chem. 2025, 64, 2926−2935

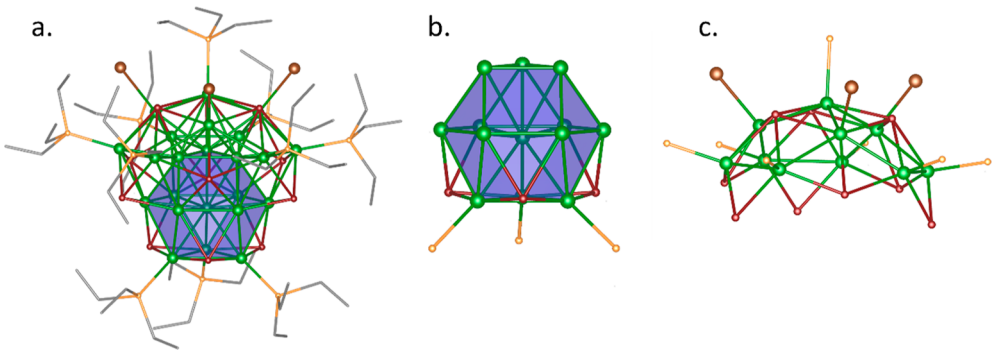

Figure 2. Ball and stick structure of $[Ni_{23}Se_{12}Br_3(PEt_3)_{10}]\cdot 2THF$ (**1-Br**·2THF). Ni atoms are shown in green, and the blue polyhedron represents the coordination sphere of the central Ni atom. P, Se, and Br atoms are shown in orange, maroon, and brown, respectively. C atoms are depicted in gray wireframe. Hydrogen atoms and THF solvate atoms are omitted for clarity. (a) **1-Br**·2THF shown perpendicular to the C_3 axis. (b) $[Ni_{13}]^{7+}$ anticuboctahedral kernel. (c) $[Ni_{10}(\mu\text{-}Se)_9Br_3]^-$ shell attached to the $[Ni_{13}]^{7+}$ kernel.

Table 1. Bond Length (Å) Comparison between 1-Cl, 1-Br, and 1-I

cluster		Ni−Ni	Ni−P	Ni−Se	Ni-X
1-Cl	average	2.56	2.21	2.38	2.270(3)
	range	2.345(3)−2.796(3)	2.199(4)−2.227(6)	2.296(2)−2.4688(19)	
1-Br	average	2.56	2.21	2.384	2.3894(15)
	range	2.3494(19)−2.829(2)	2.201(3)−2.249(5)	2.2963(15)−2.4737(14)	
1-I	average	2.57	2.22	2.386	2.5880(14), 2.617(2)
	range	2.348(2)−2.8536(19)	2.198(3)−2.281(4)	2.2915(10)−2.4802(16)	

presence is also due to halide exchange in the ESI-MS injection line.

UV−vis spectra were also collected for **1-Cl**, **1-Br**, and **1-I** in THF at room temperature (Figure 1c). The spectra for all three complexes are very similar. Each displays a shoulder at ca. 325 nm, in addition to intense, broad absorption bands at ca. 400 and 600 nm. The spectra are broadly similar to those reported for other transition metal nanoclusters.[50] Additionally, the similarity of all three spectra suggests that the observed absorptions are likely electronic transitions within the Ni_{23} core. Accordingly, it appears that halide exchange does not cause a large perturbation of the cluster electronic structure. Similar spectral behavior has been observed previously. For example, $[Au_{10}(^{MesCH2}Bimy)_6X_3]^+$ (X = Cl, Br) exhibit nearly identical UV−vis spectra,[51] as do $[Au_{13}(dppe)_5X_2]^{3+}$ (X = Cl, Br, I).[32]

To further probe the electronic structure of the Ni_{23} clusters, temperature-dependent dc magnetization data were collected for a crystalline sample of **1-Br** at H = 1000 Oe (Figure 1d). It features a room-temperature moment of $\chi_M T$ = 1.39 cm^3 K mol^{-1} (μ_{eff} = 3.34 μ_B), which drops to $\chi_M T$ = 0.43 cm^3 K mol^{-1} (μ_{eff} = 1.85 μ_B) at T = 2 K. For comparison, the spin only moment for an S = 1/2 system is 0.37 cm^3 K mol^{-1}. Overall, these data are consistent with an S = 1/2 ground state at low temperatures, with thermal population of low-lying S = 3/2 or 5/2 excited states on warming, suggesting that there is a dense manifold of orbitals near the HOMO−LUMO gap. Similar behavior is observed for $[Ni_{30}S_{16}(PEt_3)_{11}]$,[15] likely for the same reason. The room temperature moment recorded for **1-Br** in the solid state is similar to that found for **1-Cl** in CD_2Cl_2 (Evans' method: 1.58 cm^3 K mol^{-1} at 298 K),[14] suggesting that the two clusters have similar ground states. However, its magnetic moment is much higher than that reported by Steigerwald and co-workers reported for $[Ni_{23}Se_{12}(PEt_3)_{13}]$ (ca. 0.36 cm^3 K mol^{-1} at 150 K).[52] The origin of this discrepancy is currently unclear.

X-ray Crystallography. X-ray structural data were collected for clusters **1-Br** and **I-I**. In addition, we recharacterized **1-Cl** using synchrotron radiation at the advanced photon source (APS). The new data collected for **1-Cl** using synchrotron radiation was of higher quality (R_1 = 0.0404) than the data previously reported for **1-Cl** (R_1 = 0.0884),[14] which helps solidify our revised formulation of this cluster.

As previously reported,[14] **1-Cl** crystallizes in the trigonal space group $R3c$ as the THF solvate, **1-Cl**·2THF (Figure S1). Cluster **1-Br** similarly crystallizes in the trigonal space group $R3c$ as the THF solvate, $[Ni_{23}Se_{12}Br_3(PEt_3)_{10}]\cdot 2THF$ (**1-Br**·2THF) (Figure 2). Cluster **1-I** crystallizes in the monoclinic space group $P2_1/m$ as the diethyl ether solvate, $[Ni_{23}Se_{12}I_3(PEt_3)_{10}]\cdot Et_2O$ (**1-I**·Et_2O). All three clusters are isostructural. Each features a $[Ni_{13}]^{7+}$ anticuboctahedral kernel, where one hemisphere of the kernel is capped by a $[Ni_{10}(\mu\text{-}Se)_9X_3]^-$ shell. Seven PEt_3 ligands are attached to the $[Ni_{10}(\mu\text{-}Se)_9X_3]^-$ shell: six PEt_3 ligands are located along the equatorial belt, and one PEt_3 ligand is located at the apex. The other hemisphere of the $[Ni_{13}]^{7+}$ kernel is bound to three PEt_3 ligands and three $(\mu_4\text{-}Se)^{2-}$ ligands, which are arranged to form a C_3-symmetric [*cyclo*-$Ni_3(\mu\text{-}Se)_3(PEt_3)_3$] terrace. Similar terrace features are found in the related Ni APNCs, $[Ni_{30}S_{16}(PEt_3)_{11}]$ and $[Ni_{26}S_{14}(PEt_3)_{10}]$.[15] $[Ni_{30}S_{16}(PEt_3)_{11}]$ and $[Ni_{26}S_{14}(PEt_3)_{10}]$ also feature "metal-like" cores characterized by interpenetrating Ni_{13} kernels and a high degree of Ni−Ni bonding. The recently reported Fe APNC, $[(Tp^*WS_3)_4Fe_{13}]$, also features a M_{13} kernel.[9] As mentioned above, Ni APNCs are exceptionally rare. Only a handful are known, including the aforementioned $[Ni_{30}S_{16}(PEt_3)_{11}]$ and $[Ni_{26}S_{14}(PEt_3)_{10}]$, as well as $[Ni_{21}Se_{14}(PEt_2Ph)_{12}]$, $[Ni_9Te_6(PEt_3)_8]^{n+}$ (n = 0, 1, 2), and $[Ni_9Te_6(PMe_3)_8]^{n+}$ (n = 0, 1, 2).[8,14−22]

As expected, the Ni−X distances increase with the increasing halide ionic radii (**1-Cl**: 2.270(3) Å; **1-Br**: 2.3894(15) Å; **1-I**:

https://doi.org/10.1021/acs.inorgchem.4c05088
Inorg. Chem. 2025, 64, 2926−2935

2.5880(14), 2.617(2) Å).[53] Otherwise, the metrical parameters between the three clusters are very similar, consistent with their nearly identical NMR and UV−vis spectral data. For example, the average Ni−Ni distances are nearly identical (**1-Cl**: 2.56 Å, **1-Br**: 2.56 Å, **1-I**: 2.57 Å, Table 1), as are the average Ni−Se distances (**1-Cl**: 2.38 Å, **1-Br**: 2.38 Å, **1-I**: 2.39 Å). The Ni−P_{apical} distances are also nearly identical (**1-Cl**: 2.227(6) Å, **1-Br**: 2.249(5) Å, **1-I**: 2.281(4) Å), which is notable since the apical PEt_3 ligand interacts the most with the three halide ligands, further confirming the minimal disruption to the cluster structure upon halide exchange.

The average formal Ni-oxidation state in **1-X** is +1.17. While this value is indicative of a highly reduced cluster, the low symmetry of the cluster suggests that the redox load is not evenly supported by all 23 Ni centers. Indeed, given the number of Se^{2-} and X^- ligands within the $[Ni_{10}(\mu\text{-}Se)_9X_3]^-$ shell, it is likely that all 10 of these Ni centers are in the formal +2 oxidation state. Moreover, given the presence of many strong field PEt_3 and Se^{2-} ligands within the $[Ni_{10}(\mu\text{-}Se)_9X_3]^-$ shell, these 10 Ni^{2+} centers are likely low spin and diamagnetic. Accordingly, the average formal oxidation state of the nickel atoms within the $[Ni_{13}]^{7+}$ kernel is +0.54. The redox load across these 13 Ni centers is probably more evenly distributed, given the similar coordination environments among these metal atoms. However, the proposed 7+ charge of the kernel implies an odd-numbered electronic configuration, with minimum and maximum spin states of $S = 1/2$ and $S = 7/2$, respectively. The former value is consistent with observed low temperature moment of **1-Br** (Figure 1d).

Attempted Bottom-Up Syntheses of $[Ni_{23}Se_{12}X_3(PEt_3)_{10}]$. The reported bottom-up synthesis for **1-Cl** is potentially modular (Scheme 1), since a variety of X-type ligands could be introduced into the cluster by changing the identity of the NiX_2 salt used in the reaction. To test this hypothesis, we attempted to prepare the **1-Br** by substitution of $[NiCl_2(PEt_3)_2]$ with $[NiBr_2(PEt_3)_2]$. Thus, treatment of a THF solution of $[Ni(1,5\text{-cod})_2]$ (23 equiv) and PEt_3 (1 equiv) with $SePEt_3$ (17 equiv), followed by addition of $[NiBr_2(PEt_3)_2]$ (4 equiv) resulted in formation of a dark brown solution after 4 d (Scheme 2B). Workup of the reaction mixture afforded the isolation of **1-Br** as a black crystalline solid in 43% yield from the THF fraction. We were also able to isolate the Ni_3 cluster, $[Ni_3(\mu_3\text{-}Se)_2Br_2(PEt_3)_4]$ (**2-Br**), from the toluene fraction of the reaction mixture, in 26% yield. A similar byproduct was reported for the synthesis of **1-Cl**, namely, $[Ni_3(\mu_3\text{-}Se)_2Cl_2(PEt_3)_4]$ (**2-Cl**).[14] The formation of **2-Br** during the reaction partially explains the low isolated yield of **1-Br** by this route, since it sequesters equivalents of both Br and Ni. Additionally, we found the purity of **1-Br** was improved by addition of 4 equiv of $[NiBr_2(PEt_3)_2]$, instead of the 1.5 equiv suggested by the idealized reaction stoichiometry. While this change likely increases the yield of **2-Br**, it reduced the amount of adventitious chloride observed in isolated samples of **1-Br**.

We also attempted the bottom-up synthesis of **1-I**, using the same conditions employed to make **I-Cl** and **I-Br**. Thus, treatment of a THF solution of $[Ni(1,5\text{-cod})_2]$ (23 equiv) and PEt_3 (1 equiv) with $SePEt_3$ (17 equiv) and then $[NiI_2(PEt_3)_2]$ (4 equiv) resulted in formation of a dark brown solution after 4 d. An ESI-mass spectrum of the crude reaction mixture (recorded in positive ion mode) reveals a complex reaction mixture (Figure S41). The mass spectrum features major peaks at 1051.20 m/z and 2241.29 m/z, which are assignable to $[Ni_3Se_2I(PEt_3)_5]^+$ ($[\mathbf{2\text{-}I} - I + PEt_3]^+$) (calcd = 1051.00 m/z) and $[Ni_{14}Se_9(PEt_3)_6]^+$ (calcd = 2240.88 m/z). Additionally, we observe minor peaks at 2365.4021, 3380.7861, and 3498.8943 m/z. These peaks correspond to Ni-containing clusters, but they remain unassigned. Finally, a very minor peak is observed at 3859.8368 m/z, which is assignable to $[Ni_{23}Se_{12}I_3(PEt_3)_{10}]^+$ ($[\mathbf{1\text{-}I}]^+$) (calcd m/z = 3859.1121), but given its intensity, **1-I** is clearly a minor product in the reaction mixture. The ^1H NMR spectrum of the crude reaction mixture in C_6D_6 reveals that **2-I** is the major reaction product (Figure S19), consistent with the ESI-MS results. However, a number of other species are also present in the reaction mixture, as indicated by additional resonances between 33.8 and 40.7 ppm. Given the apparent paramagnetism of these products, we suggest they correspond to the unidentified Ni-containing clusters observed in the ESI-MS spectrum. We also observe minor peaks at 38.19, 8.19, 5.15, and 3.07 ppm, which are assignable to **1-I**. Complexes **2-I** and **1-I** are present in a 20:1 ratio in this sample, according to integration of the ^1H NMR spectrum. Given the trace formation of **1-I** in the reaction mixture, this approach is clearly not synthetically useful.

To explain the different bottom-up reaction outcome in the case of iodide, we hypothesize that the relative stability of **1-I** is much lower than that of **2-I** and the other observed cluster products. As a result, these unwanted products are favored in the cluster assembly process, resulting in lower yields of **1-I** in comparison to the analogous chloride and bromide reactions. Attempts to favor formation of **1-I**, and suppress formation of **2-I**, also failed. For example, reducing the amount of $SePEt_3$ in the reaction mixture still resulted in formation of **2-I** as the major product, while **1-I** is no longer observed in the reaction mixture. These failed efforts to suppress the formation of **2-I** demonstrate its inherent stability, and further emphasize the importance of postsynthetic modification in the isolation of **1-I**.

CONCLUSIONS

We have synthesized two new nickel APNCs, $[Ni_{23}Se_{12}X_3(PEt_3)_{10}]$ (X = Br, I). While the bromide analogue could be made by two routes: postsynthetic ligand exchange and bottom-up synthesis; the iodide analogue could only be made by postsynthetic ligand exchange. Attempts to make $[Ni_{23}Se_{12}I_3(PEt_3)_{10}]$ via bottom-up synthesis instead resulted in formation of $[Ni_3(\mu_3\text{-}Se)_2I_2(PEt_3)_4]$ as the major product, suggesting that the Ni_3 cluster features enhanced stability relative to the target APNC. This work highlights the challenges inherent in the bottom-up synthesis of Ni APNCs: while $[Ni_{23}Se_{12}I_3(PEt_3)_{10}]$ is thermodynamically stable, as evidenced by its isolation and characterization, it is clearly kinetically inaccessible via the bottom-up reaction pathway. Overall, our findings demonstrate the value of postsynthetic modification toward the synthesis of Ni APNCs, which have proven difficult to synthesize by bottom-up methods. Easier access to new Ni APNCs will enable new technological uses for these materials, including for catalysis and magnetism applications.

EXPERIMENTAL SECTION

General Procedures. All operations were performed in a glovebox under an atmosphere of N_2, unless otherwise noted. Hexanes, diethyl ether, and toluene were dried by passage over activated molecular sieves using a Vacuum Atmospheres DRI-SOLV solvent purification system, and stored over activated 3 Å molecular

https://doi.org/10.1021/acs.inorgchem.4c05088
Inorg. Chem. 2025, 64, 2926−2935

sieves for 24 h prior to use. Pentane was dried on an MBraun solvent purification system and stored over activated 3 Å molecular sieves for 24 h prior to use. THF was first distilled from calcium hydride, then distilled from Na/benzophenone and stored over activated 3 Å molecular sieves for 24 h prior to use. C_6D_6 was dried over activated 3 Å molecular sieves for 48 h prior to use. $[Ni_{23}Cl_3Se_{12}(PEt_3)_{10}]$ (**1-Cl**) was prepared according to published literature procedures.[14] *Bis*(1,5-cyclooctadiene)nickel(0) (98+%) was purchased from Strem chemicals and used as received. Triethylphosphine, 99%, was purchased from Sigma-Aldrich and used as received. Selenium powder, −200 mesh, 99.999% (metals basis) was purchased from Alfa Aesar and used as received. Triethylphosphine selenide was prepared by reaction of PEt_3 with Se powder in toluene.[17,54] The resulting solution was filtered, layered with hexanes, and stored at −25 °C for 24 h, which resulted in the deposition of colorless needles. These needles had $^{31}P\{^1H\}$ NMR spectroscopic parameters that matched those previously described for this material.[54,55] $[NiX_2(PEt_3)_2]$ (X = Br, I) were prepared by heating a mixture of anhydrous NiX_2 and PEt_3 (2 equiv) in THF at 65 °C in a Cajon flask for 17 h. The resulting solutions were filtered through a Celite column supported on glass wool (0.5 cm × 5 cm) to afford purple (X = Br) or green (X = I) filtrates. The filtrates were concentrated in vacuo, layered with hexanes, and stored at −25 °C for 2 d, which resulted in the deposition of red-purple blocks of $[NiBr_2(PEt_3)_2]$ or dark green blocks of $[NiI_2(PEt_3)_2]$. These solids matched the descriptions previously reported for these materials.[56,57] All other reagents were purchased from commercial suppliers and used as received.

Caution! Triethylphosphine is air-sensitive and potentially pyrophoric. It must be handled under an inert atmosphere.

All NMR spectra were collected at room temperature unless otherwise specified. ^1H, $^{13}C\{^1H\}$, and $^{31}P\{^1H\}$ NMR spectra were recorded on a Bruker AVANCE NEO 500 MHz spectrometer or a Bruker AVANCE III HD 400 MHz spectrometer. ^1H and $^{13}C\{^1H\}$ NMR spectra were referenced to external $SiMe_4$ using residual protio solvent resonances as internal standards. $^{31}P\{^1H\}$ NMR spectra were referenced indirectly to the ^1H chemical shifts of $SiMe_4$ at 0 ppm. IR spectra were recorded on a Nicolet 6700 FT-IR spectrometer. Mass spectra were collected at the Materials Research Laboratory Shared Experimental Facilities at UCSB, using an electrospray ionization (ESI) source in positive ion mode with a Waters Xevo G2-XS TOF Time-of-Flight mass spectrometer. Model mass spectra were generated in MassLynx V4.1 software with the isotope clusters displayed with a minimum abundance of 0.1%. Elemental analyses were performed by the Microanalytical Laboratory at the University of California, Berkeley, using a PerkinElmer 2400 Series II combustion analyzer. UV−vis spectra were recorded on a Shimadzu UV3600 Spectrometer.

Magnetism Measurements. Magnetic properties were recorded using a Quantum Design Magnetic Property Measurement System SQUID vibrating sample magnetometer (MPMS3 SQUID-VSM). 10−13 mg samples of polycrystalline **1-Br** were loaded into a polypropylene capsule under inert atmosphere. Melted eicosane wax (3−6 mg) was subsequently added onto the sample to minimize particle torquing during measurements, whereupon the polypropylene capsule was sealed with vacuum grease to prevent exposure to air. DC magnetic measurements were performed in VSM mode while sweeping the temperature at controlled rates. For the magnetic susceptibility measurements, diamagnetic corrections for **1-Br** (χ_{dia} = −20.18 × 10^{-4} cm^3/mol) and eicosane (χ_{dia} = −2.43 × 10^{-4} cm^3/mol) were made using Pascal's constants. The data were not corrected for the contribution from the sample holder and vacuum grease.

Synthesis of $[Ni_{23}Se_{12}Br_3(PEt_3)_{10}]$ (1-Br) via Halide Metathesis. A 20 mL scintillation vial equipped with a magnetic stir bar was charged with $[Ni_{23}Se_{12}Cl_3(PEt_3)_{10}]$ (**1-Cl**) (0.023 g, 0.006 mmol) and THF (4 mL). Me_3SiBr (2.5 μL, 0.019 mmol) was added via microsyringe to the stirring solution. This solution was stirred for 30 min at room temperature, whereupon the volatiles were removed in vacuo. The resulting black solid was triturated with pentane (1 mL × 2). The dark brown product was then rinsed with toluene (3 mL) and the rinsings were discarded. The remaining solid was dissolved in THF (3 mL), and filtered through the Celite column supported on glass wool (0.5 cm × 5 cm). The dark brown filtrate was layered with hexanes (6 mL) and stored at −25 °C for 48 h, which resulted in the deposition of black blocks. The blocks were isolated by decanting the supernatant, rinsing with hexanes (2 mL), and drying in vacuo (15.3 mg, 64% yield). ^1H NMR (400 MHz, 25 °C, C_6D_6): δ 43.45 (br s, CH_2CH_3, 6H), 7.11 (br s, CH_2CH_3, 9H), 5.51 (m, J_{HH} = 7.2 Hz, CH_2CH_3, 18H, diastereotopic), 5.36 (m, J_{HH} = 7.2 Hz, CH_2CH_3, 18H, diastereotopic), 3.38 (m, J_{HH} = 7.3 Hz, CH_2CH_3, 18H), 1.83 (m, CH_2CH_3, 54H), 1.15 (m, CH_2CH_3, 27H). ESI-MS (THF, positive ion mode, 3.00 kV): 3719.33 *m/z* ($[Ni_{23}Se_{12}Br_3(PEt_3)_{10}]^+$ ($[\mathbf{1\text{-}Br}]^+$), calcd 3719.15 *m/z*), 3675.37 *m/z* ($[Ni_{23}Se_{12}Br_2Cl(PEt_3)_{10}]^+$ ($[\mathbf{1\text{-}Br} - Br + Cl]^+$), calcd 3673.20 *m/z*), 3638.41 *m/z* ($[Ni_{23}Se_{12}Br_2(PEt_3)_{10}]^+$ ($[\mathbf{1\text{-}Br} - Br]^+$), calcd 3638.25 *m/z*).

Bottom-Up Synthesis of $[Ni_{23}Se_{12}Br_3(PEt_3)_{10}]$ (1-Br). A 20 mL scintillation vial equipped with a magnetic stir bar was charged with $[Ni(1,5\text{-cod})_2]$ (0.152 g, 0.554 mmol), THF (10 mL) and PEt_3 (3.5 μL, 0.024 mmol). Crystalline $SePEt_3$ (0.081 g, 0.412 mmol) was then added as a solid to the stirring solution. This solution was stirred at room temperature for 15 min, whereupon the pale-yellow solution turned brown. $[NiBr_2(PEt_3)_2]$ (0.043 g, 0.095 mmol) and THF (2 mL) were then added separately to this solution. The solution was allowed to stir for 4 d at room temperature, whereupon all volatiles were removed in vacuo. The resulting brown waxy solid was triturated with pentane (1 mL × 2), and then rinsed with pentane (4 mL), diethyl ether (4 mL), toluene (8 mL), and THF (10 mL). Each of these rinsings were filtered through a Celite column supported on glass wool (0.5 cm × 5 cm), furnishing dark brown filtrates in each case. The pentane and diethyl ether filtrates were discarded. The toluene filtrate was layered with hexanes (8 mL) and stored at −25 °C for 72 h, which resulted in the deposition of $[Ni_3(\mu_3\text{-}Se)_2(PEt_3)_4]$ (**2-Br**) as a black crystalline solid (0.047 g, 26% yield by $[Ni(1,5\text{-cod})_2]$). The solid was isolated by decanting the supernatant and rinsing the crystalline material with hexanes (2 mL). The crystals were then dried in vacuo and their identity was confirmed via ^1H and $^{31}P\{^1H\}$ NMR spectroscopy (Figures S24 and S25). ^1H NMR (400 MHz, 25 °C, C_6D_6): δ 1.80−1.62 (m, CH_2CH_3, 12H), 1.60−1.44 (m, CH_2CH_3, 12H), 1.33 (m, J_{HP} = 15.2 Hz, J_{HH} = 7.5 Hz, CH_2CH_3, 18H), 1.12 (m, J_{HP} = 15.9 Hz, J_{HH} = 7.5 Hz, CH_2CH_3, 18H). $^{31}P\{^1H\}$ NMR (162 MHz, 25 °C, C_6D_6): δ 14.63 (m, J_{PP} = 10.5 Hz, 2P), 13.72 (m, J_{PP} = 10.5 Hz, 2P).

The above-mentioned THF filtrate was layered with hexanes (10 mL) and stored at −25 °C for 72 h, which resulted in the deposition of **1-Br** as a black crystalline solid (0.039 g, 43% yield by $[Ni(1,5\text{-cod})_2]$). The solid was collected by decanting the pale brown supernatant and rinsing the crystalline solids with hexanes (1 mL × 3). Crystals grown in this manner were suitable for single crystal X-ray diffraction. Anal. Calcd for $C_{68}H_{166}O_2Br_3Ni_{23}P_{10}Se_{12}$: C, 21.14; H, 4.33. Found: C, 20.97; H, 4.50. ^1H NMR (500 MHz, 25 °C, C_6D_6): δ 43.50 (br s, CH_2CH_3, 6H), 7.12 (br s, CH_2CH_3, 9H), 5.53 (m, J_{HH} = 6.9 Hz, CH_2CH_3, 18H, diastereotopic), 5.37 (m, J_{HH} = 6.9 Hz, CH_2CH_3, 18H, diastereotopic), 3.40 (m, J_{HH} = 7.0 Hz, CH_2CH_3, 18H), 1.83 (m, CH_2CH_3, 54H), 1.15 (m, CH_2CH_3, 27H). $^1H\{^{31}P\}$ NMR (500 MHz, 25 °C, C_6D_6): δ 43.47 (br s, CH_2CH_3, 6H), 7.12 (br s, CH_2CH_3, 9H), 5.51 (m, J_{HH} = 6.9 Hz, CH_2CH_3, 18H, diastereotopic), 5.36 (m, J_{HH} = 6.9 Hz, CH_2CH_3, 18H, diastereotopic), 3.38 (m, J_{HH} = 7.0 Hz, CH_2CH_3, 18H), 1.83 (m, CH_2CH_3, 54H), 1.15 (m, CH_2CH_3, 27H). $^{31}P\{^1H\}$ NMR (203 MHz, 25 °C, C_6D_6): δ 434 (br s, 3P), 1035 (br s, 6P). ESI-MS (THF, positive ion mode, 2.50 kV): 3720.67 *m/z* ($[Ni_{23}Se_{12}Br_3(PEt_3)_{10}]^+$ ($[\mathbf{1\text{-}Br}]^+$), calcd 3719.15 *m/z*), 3674.65 *m/z* ($[Ni_{23}Se_{12}Br_2Cl(PEt_3)_{10}]^+$ ($[\mathbf{1\text{-}Br} - Br + Cl^+$), calcd 3673.20 *m/z*). FT-IR (cm^{-1}): 449 (w), 619 (m), 711 (s), 732 (s), 768 (s), 997 (m), 1031 (s), 1126 (s), 1247 (m), 1274 (w), 1377 (w), 1411 (m), 1457 (m), 2875 (m), 2930 (m), 2968 (m). UV−vis (THF, 0.038 mM, 25 °C, L mol^{-1} cm^{-1}): 325 nm (sh, ε = 47,000), 401 nm (ε = 51,000), 616 nm (ε = 12,000).

Synthesis of $[Ni_3(\mu_3\text{-}Se)_2Br_2(PEt_3)_4]$ (2-Br). A 20 mL scintillation vial equipped with a magnetic stir bar was charged with $[Ni(1,5\text{-cod})_2]$ (0.093 g, 0.337 mmol), $SePEt_3$ (0.090 g, 0.457 mmol), and

https://doi.org/10.1021/acs.inorgchem.4c05088
Inorg. Chem. 2025, 64, 2926−2935

THF (4 mL). This solution was stirred for 20 min, whereupon the pale-yellow solution turned brown. To this solution, $[NiBr_2(PEt_3)_2]$ (0.076 g, 0.167 mmol) was added as a solid. Upon the addition of $[NiBr_2(PEt_3)_2]$, the solution became deep brown. The solution was allowed to stir for 2 d at room temperature, whereupon the volatiles were removed in vacuo. The resulting black solid was triturated with pentane (1 mL × 2), suspended in diethyl ether (4 mL), and filtered through a Celite column supported on glass wool (0.5 cm × 5 cm), furnishing a brown filtrate. The remaining solids were dissolved in toluene (4 mL) and filtered through the same Celite column, furnishing a brown filtrate. The Et_2O fraction was discarded. The toluene fraction was layered with hexanes (15 mL), and stored at −25 °C which resulted in the deposition of black blocks. The crystals were isolated by decanting the supernatant, rinsing with hexanes (3 mL), and drying in vacuo to give **2-Br** (0.085 g, 78% yield). Anal. Calcd for $C_{24}H_{60}Br_2Ni_3P_4Se_2$: C, 29.83; H, 6.26. Found: C, 30.06; H, 6.28. ^{1}H NMR (500 MHz, 25 °C, C_6D_6): δ 1.81−1.62 (m, CH_2CH$_3$, 12H), 1.60−1.45 (m, CH_2CH$_3$, 12H), 1.33 (m, J_{HP} = 15.2 Hz, J_{HH} = 7.5 Hz, CH$_2$CH_3, 18H), 1.12 (m, J_{HP} = 15.9 Hz, J_{HH} = 7.5 Hz, CH$_2$CH_3, 18H). ^{31}P{^{1}H} NMR (202 MHz, 25 °C, C_6D_6): δ 14.63 (m, J_{PP} = 10.1 Hz, 2P), 13.74 (m, J_{PP} = 10.1 Hz, 2P). ^{13}C{^{1}H} NMR (126 MHz, 25 °C, C_6D_6): δ 18.38−18.18 (m, J_{CP} = 25.8 Hz, CH_2CH$_3$), 16.81−16.61 (m, J_{CP} = 25.0 Hz, CH_2CH$_3$), 8.84 (s, CH$_2$CH_3), 8.62 (s, CH$_2$CH_3). FT-IR (cm^{-1}): 417 (m), 625 (m), 719 (s), 766 (s), 998 (m), 1034 (s), 1125 (w), 1244 (m), 1375 (w), 1412 (m), 1454 (m), 2355 (w), 2876 (m), 2904 (m), 2931 (m), 2957 (m).

Synthesis of $[Ni_{23}Se_{12}I_3(PEt_3)_{10}]$ (1-I) via Halide Metathesis. A 20 mL scintillation vial equipped with a magnetic stir bar was charged with $[Ni_{23}Se_{12}Cl_3(PEt_3)_{10}]$ (**1-Cl**) (0.050 g, 0.014 mmol) and THF (4 mL). Me_3SiI (16 μL, 0.084 mmol) was then added via microsyringe to the stirring solution. This solution was stirred for 1.5 h at room temperature, whereupon the volatiles were removed in vacuo. The resulting black solid was triturated with pentane (1 mL × 2) and then rinsed with diethyl ether (2 mL). The rinsings were filtered through a Celite column supported on glass wool (0.5 cm × 5 cm), furnishing a brown filtrate, which was discarded. The remaining solids were dissolved in toluene (3 mL), and filtered through the same Celite column, furnishing a brown filtrate. The toluene fraction was layered with hexanes (8 mL) and stored at −25 °C for 48 h, which resulted in the deposition of black blocks. The crystals were isolated by decanting the supernatant. The crystals were then rinsed with hexanes (2 mL) and dried in vacuo to give **1-I** (36 mg, 67% yield). X-ray quality crystals were grown from concentrated diethyl ether. Anal. Calcd for $C_{60}H_{150}I_3Ni_{23}P_{10}Se_{12}$: C, 18.67; H, 3.92. Found: C, 19.00; H, 3.83. ^{1}H NMR (500 MHz, 25 °C, C_6D_6): δ 38.2 (br s, CH_2CH$_3$, 6H), 8.19 (br s, CH$_2$CH_3, 9H), 5.15 (m, CH_2CH$_3$, 36H), 3.09 (m, CH_2CH$_3$, 18H), 1.85 (m, CH$_2$CH_3, 54H), 1.11 (m, CH$_2$CH_3, 27H). ^{31}P{^{1}H} NMR (202 MHz, 25 °C, C_6D_6): δ 362 (br s, 3P), 942 (br s, 6P). ESI-MS (THF, positive ion mode, 3.00 kV): 3859.67 m/z ($[Ni_{23}Se_{12}I_3(PEt_3)_{10}]^+$ ([**1-I**]$^+$), calcd 3859.11 m/z), 3813.66 m/z ($[Ni_{23}Se_{12}I_2Br(PEt_3)_{10}]^+$ ([**1-I** − I + Br]$^+$), calcd 3813.10 m/z), 3767.68 m/z ($[Ni_{23}Se_{12}I_2Cl(PEt_3)_{10}]^+$ ([**1-I** − I + Cl]$^+$), calcd 3769.20 m/z). FT-IR (cm^{-1}): 418 (w), 450 (w), 618(w), 668 (m), 711 (s), 732 (s), 735 (s), 766 (s), 998 (m), 1032 (s), 1129 (s), 1248 (w), 1280 (w), 1376 (w), 1409 (m), 1457 (m), 2333 (w), 2364 (w), 2876 (m), 2900 (m), 2929 (m), 2963 (m). UV−vis (THF, 0.050 mM, 25 °C, L mol^{-1} cm^{-1}): 325 nm (sh, ε = 50,000), 399 nm (ε = 53,000), 619 nm (ε = 13,000).

Attempted Bottom-Up Synthesis of $[Ni_{23}Se_{12}I_3(PEt_3)_{10}]$ (1-I). A 20 mL scintillation vial equipped with a magnetic stir bar was charged with $[Ni(1,5\text{-cod})_2]$ (0.134 g, 0.487 mmol) and THF (10 mL). To this suspension was added PEt_3 (3.1 μL, 0.021 mmol) via microsyringe. Crystalline $SePEt_3$ (0.070 g, 0.355 mmol) was then added as a solid to the stirring solution. This solution was stirred at room temperature for 15 min, whereupon the pale-yellow solution turned brown. $[NiI_2(PEt_3)_2]$ (0.048 g, 0.087 mmol) and THF (2 mL) were then added separately to this solution. The solution was allowed to stir for 4 d at room temperature, whereupon an aliquot was removed and dried in vacuo, redissolved in C_6D_6 (0.75 mL), and filtered through a Celite column supported on glass wool (0.5 cm × 4 cm) into an NMR tube for NMR analysis. An additional aliquot was taken for ESI-MS analysis. The ^{1}H and ^{31}P NMR spectra (Figures S19 and S20) and ESI-mass spectrum (in positive ion mode) (Figure S41) reveal a mixture of products. The ^{1}H and ^{31}P NMR spectra contain peaks assignable to **2-I**, **1-I**, and other unidentified paramagnetic products. The ESI-mass spectrum features peaks assignable to [**2-I** − I + PEt_3]$^+$ and $[Ni_{14}Se_9(PEt_3)_6]^+$ as major products, and a peak assignable to [**1-I**]$^+$ as a minor product. ^{1}H NMR (400 MHz, 25 °C, C_6D_6): δ 40.7 (br s, unassigned), 38.2 (br s, **1-I**), 33.8 (br s, unassigned), 8.19 (br s, **1-I**), 5.58 (s, cyclooctadiene), 5.15 (br s, **1-I**), 3.58 (s, THF), 3.07 (s, **1-I**), 2.21 (s, cyclooctadiene), 1.91−1.71 (m, **2-I**), 1.57−1.41 (m, **2-I**), 1.30 (m, **2-I**), 1.08 (m, **2-I**), 0.86 (m, $SePEt_3$). ^{31}P{^{1}H} NMR (162 MHz, 25 °C, C_6D_6): δ 939 (br s, **1-I**), 360 (br s, **1-I**), 42.90 (s, $SePEt_3$), 17.23 (br s, **2-I**), 16.31 (br s, **2-I**). ESI-MS (THF, positive ion mode, 2.00 kV): 3861.98 m/z ($[Ni_{23}Se_{12}I_3(PEt_3)_{10}]^+$ ([**1-I**]$^+$), calcd 3859.11 m/z), 3498.89 m/z (unassigned), 3380.78 m/z (unassigned), 2365.40 m/z (unassigned), 2241.29 m/z ($[Ni_{14}Se_9(PEt_3)_6]^+$, calcd 2240.90 m/z), 1051.20 m/z ($[Ni_3Se_2I(PEt_3)_5]^+$ ([**2-I** − I + PEt_3]$^+$), calcd 1052.99 m/z).

The remaining reaction mixture was dried in vacuo. The resulting brown waxy solid was triturated with pentane (1 mL × 2), and then rinsed with pentane (4 mL). The pentane filtrate was discarded. The remaining solid were then rinsed with diethyl ether (4 mL) and toluene (6 mL), and each fraction was filtered through a Celite column supported on glass wool (0.5 cm × 5 cm), furnishing dark brown filtrates. The diethyl ether filtrate was discarded. The toluene filtrate was layered with hexanes (8 mL) and stored at −25 °C for 48 h, which resulted in the deposition of black solid. The solid was isolated by decanting the supernatant. The crystals were then rinsed with hexanes (2 mL) and dried in vacuo to give $[Ni_3(\mu_3\text{-}Se)_2I_2(PEt_3)_4]$ (**2-I**) (0.028 g, 16% yield by $[Ni(1,5\text{-cod})_2]$). ^{1}H NMR (400 MHz, 25 °C, C_6D_6): δ 1.92−1.71 (m, CH_2CH$_3$, 12H), 1.57−1.41 (m, CH_2CH$_3$, 12H), 1.30 (m, J_{HP} = 14.8 Hz, J_{HH} = 7.5 Hz, CH$_2$CH_3, 18H), 1.08 (m, J_{HP} = 14.8 Hz, J_{HH} = 7.5 Hz, CH$_2$CH_3, 18H). ^{31}P{^{1}H} NMR (162 MHz, 25 °C, C_6D_6): δ 17.23 (br s, 2P), 16.30 (br s, 2P).

Synthesis of $[Ni_3(\mu_3\text{-}Se)_2I_3(PEt_3)_4]$ (2-I). A 20 mL scintillation vial equipped with a magnetic stir bar was charged with $[Ni(1,5\text{-cod})_2]$ (0.075 g, 0.273 mmol) and THF (5 mL). A THF (2 mL) solution of $SePEt_3$ (0.073 g, 0.370 mmol) was then added to the stirring solution. This solution was stirred for 20 min, whereupon the pale-yellow solution turned brown. To this solution, $[NiI_2(PEt_3)_2]$ (0.076 g, 0.138 mmol) was added as a solid, which resulted in a color change to deep brown. The solution was allowed to stir for 2 d at room temperature, whereupon the volatiles were removed in vacuo. The resulting black solid was triturated with pentane (1 mL × 2). The dark brown product was suspended in diethyl ether (2 mL) and filtered through a Celite column supported on glass wool (0.5 cm × 5 cm), furnishing a brown filtrate. The diethyl ether rinsings were discarded. The remaining solids were dissolved in toluene (4 mL) and filtered through the same Celite column, furnishing a brown filtrate. The toluene fraction was layered with hexanes (10 mL), and stored at −25 °C for 48 h, which resulted in the deposition of black blocks. The solid was isolated by decanting the supernatant, rinsing with hexanes (3 mL), and drying in vacuo to give **2-I** (0.049 g, 51% yield). Anal. Calcd for $C_{24}H_{60}I_2Ni_3P_4Se_2$: C, 27.18; H, 5.70. Found: C, 27.47; H, 5.71. ^{1}H NMR (500 MHz, 25 °C, C_6D_6): δ 1.93−1.69 (m, CH_2CH$_3$, 12H), 1.59−1.40 (m, CH_2CH$_3$, 12H), 1.30 (m, J_{HP} = 15.0 Hz, J_{HH} = 7.6 Hz, CH$_2$CH_3, 18H), 1.09 (m, J_{HP} = 15.3 Hz, J_{HH} = 7.7 Hz, CH$_2$CH_3, 18H). ^{31}P{^{1}H} NMR (202 MHz, 25 °C, C_6D_6): δ 17.22 (m, J_{PP} = 12.1 Hz, 2P), 16.31 (m, J_{PP} = 12.1 Hz, 2P). ^{13}C{^{1}H} NMR (126 MHz, 25 °C, C_6D_6): δ 18.30−17.96 (m, overlapping CH$_2$CH$_3$), 9.00 (s, CH$_2$CH$_3$), 8.64 (s, CH$_2$CH$_3$). FT-IR (cm^{-1}): 419 (m), 628 (m), 715 (s), 763 (s), 996 (m), 1033 (s), 1114 (w), 1244 (m), 1374 (m), 1409 (m), 1448 (m), 2334 (w),2360 (w), 2869 (m), 2903 (m), 2925(m), 2954 (m).

https://doi.org/10.1021/acs.inorgchem.4c05088
Inorg. Chem. 2025, 64, 2926−2935

■ ASSOCIATED CONTENT

Supporting Information

The Supporting Information is available free of charge at https://pubs.acs.org/doi/10.1021/acs.inorgchem.4c05088.

Additional experimental procedures and crystallographic, spectroscopic, and magnetic characterization details for **1-X** and **2-X** (PDF)

Accession Codes

Deposition Numbers 2387159−2387163 contain the supplementary crystallographic data for this paper. These data can be obtained free of charge via the joint Cambridge Crystallographic Data Centre (CCDC) and Fachinformationszentrum Karlsruhe Access Structures service.

■ AUTHOR INFORMATION

Corresponding Author

Trevor W. Hayton − *Department of Chemistry and Biochemistry, University of California Santa Barbara, Santa Barbara, California 93106, United States;* orcid.org/0000-0003-4370-1424; Email: hayton@chem.ucsb.edu

Authors

Phoebe R. Hertler − *Department of Chemistry and Biochemistry, University of California Santa Barbara, Santa Barbara, California 93106, United States*

Alexander J. Touchton − *Department of Chemistry and Biochemistry, University of California Santa Barbara, Santa Barbara, California 93106, United States*

Guang Wu − *Department of Chemistry and Biochemistry, University of California Santa Barbara, Santa Barbara, California 93106, United States*

Tieyan Chang − *NSF's ChemMatCARS, University of Chicago, Argonne, Illinois 60439, United States;* orcid.org/0000-0002-7434-3714

Ying-Pin Chen − *NSF's ChemMatCARS, University of Chicago, Argonne, Illinois 60439, United States*

Yu-Sheng Chen − *NSF's ChemMatCARS, University of Chicago, Argonne, Illinois 60439, United States*

Complete contact information is available at: https://pubs.acs.org/10.1021/acs.inorgchem.4c05088

Notes

The authors declare no competing financial interest.

■ ACKNOWLEDGMENTS

The authors thank the National Science Foundation (CHE 2055063) for financial support of this work. This research made use of a 400 MHz NMR spectrometer supported in part by the NIH Shared Instrumentation Grant, S10OD012077. The MRL Shared Experimental Facilities are supported by the MRSEC Program of the National Science Foundation under award NSF DMR 1720256, a member of the NSF-funded Materials Research Facilities Network. NSF's ChemMatCARS, Sector 15 at the Advanced Photon Source (APS), Argonne National Laboratory (ANL) is supported by the Divisions of Chemistry (CHE) and Materials Research (DMR), National Science Foundation, under grant numbers NSF/CHE-1834750 and NSF/CHE-2335833. This research used resources of the Advanced Photon Source; a U.S. Department of Energy (DOE) Office of Science user facility operated for the DOE Office of Science by Argonne National Laboratory under contract no. DE-AC02-06CH11357.

■ REFERENCES

(1) Doud, E. A.; Voevodin, A.; Hochuli, T. J.; Champsaur, A. M.; Nuckolls, C.; Roy, X. Superatoms in materials science. *Nature Rev. Mater.* **2020**, *5*, 371−387.

(2) Jin, R.; Li, G.; Sharma, S.; Li, Y.; Du, X. Toward Active-Site Tailoring in Heterogeneous Catalysis by Atomically Precise Metal Nanoclusters with Crystallographic Structures. *Chem. Rev.* **2021**, *121*, 567−648.

(3) Gaita-Ariño, A.; Luis, F.; Hill, S.; Coronado, E. Molecular spins for quantum computation. *Nat. Chem.* **2019**, *11*, 301−309.

(4) Lisnard, L.; Tuna, F.; Candini, A.; Affronte, M.; Winpenny, R. E. P.; McInnes, E. J. L. Supertetrahedral and Bi-supertetrahedral Cages: Synthesis, Structures, and Magnetic Properties of Deca- and Enneadecametallic Cobalt(II) Clusters. *Angew. Chem., Int. Ed.* **2008**, *47*, 9695−9699.

(5) Tejada, J.; Chudnovsky, E. M.; del Barco, E.; Hernandez, J. M.; Spiller, T. P. Magnetic qubits as hardware for quantum computers. *Nanotechnology* **2001**, *12*, 181−186.

(6) Takano, S.; Tsukuda, T. Chemically Modified Gold/Silver Superatoms as Artificial Elements at Nanoscale: Design Principles and Synthesis Challenges. *J. Am. Chem. Soc.* **2021**, *143*, 1683−1698.

(7) Liu, L.; Corma, A. Metal Catalysts for Heterogeneous Catalysis: From Single Atoms to Nanoclusters and Nanoparticles. *Chem. Rev.* **2018**, *118*, 4981−5079.

(8) Hayton, T. W., Atomically Precise Nanoclusters of Iron, Cobalt, and Nickel: Why are They So Rare? In *Atomically Precise Nanochemistry*, Jin, R.; Jiang, D.-e., Eds. Wiley: 2023; 285-307.

(9) Scott, A. G.; Alves Galico, D.; Bogacz, I.; Oyala, P. H.; Yano, J.; Suturina, E. A.; Murugesu, M.; Agapie, T. High-Spin and Reactive Fe_{13} Cluster with Exposed Metal Sites. *Angew. Chem., Int. Ed.* **2023**, *62*, No. e202313880.

(10) Ebner, A.; Wachter, J.; Zabel, M. Synthesis and Characterization of Cobalttelluride Clusters with the Cubic Body-Centered $Co_9Te_6(CO)_8$ Core. *J. Cluster Sci.* **2004**, *15*, 163−174.

(11) Brunner, H.; Lucas, D.; Monzon, T.; Mugnier, Y.; Nuber, B.; Stubenhofer, B.; Stückl, A. C.; Wachter, J.; Wanninger, R.; Zabel, M. Metal Telluride Clusters Composed of Niobocene Carbonyl, Telluride, and Cobalt Carbonyl Units: Syntheses, Structures, and Reactivity. *Chem.—Eur. J.* **2000**, *6*, 493−503.

(12) Bencharif, M.; Cador, O.; Cattey, H.; Ebner, A.; Halet, J.-F.; Kahlal, S.; Meier, W.; Mugnier, Y.; Saillard, J.-Y.; Schwarz, P.; Trodi, F. Z.; Wachter, J.; Zabel, M. Electron-Sponge Behavior, Reactivity and Electronic Structures of Cobalt-Centered Cubic $Co_9Te_6(CO)_8$ Clusters. *Eur. J. Inorg. Chem.* **2008**, *2008*, 1959−1968.

(13) Wix, P.; Kostakis, G. E.; Blatov, V. A.; Proserpio, D. M.; Perlepes, S. P.; Powell, A. K. A Database of Topological Representations of Polynuclear Nickel Compounds. *Eur. J. Inorg. Chem.* **2013**, *2013*, 520−526.

(14) Touchton, A. J.; Wu, G.; Hayton, T. W. $[Ni_{23}Se_{12}(PEt_3)_{13}]$ Revisited: Isolation and Characterization of $[Ni_{23}Se_{12}Cl_3(PEt_3)_{10}]$. *Inorg. Chem.* **2021**, *60*, 17586−17592.

(15) Touchton, A. J.; Wu, G.; Hayton, T. W. $[Ni_{30}S_{16}(PEt_3)_{11}]$: an open-shell nickel sulfide nanocluster with a "metal-like" core. *Chem. Sci.* **2022**, *13*, 5171−5175.

(16) Brennan, J. G.; Siegrist, T.; Stuczynski, S. M.; Steigerwald, M. L. The transition from molecules to solids: molecular syntheses of $Ni_9Te_6(PEt_3)_8$, $Ni_{20}Te_{18}(PEt_3)_{12}$ and NiTe. *J. Am. Chem. Soc.* **1989**, *111*, 9240−9241.

(17) Brennan, J. G.; Siegrist, T.; Kwon, Y. U.; Stuczynski, S. M.; Steigerwald, M. L. Nickel-selenium-triethylphosphine $(Ni_{23}Se_{12}(PEt_3)_{13})$, an intramolecular intergrowth of nickel selenide (NiSe) and nickel. *J. Am. Chem. Soc.* **1992**, *114*, 10334−10338.

(18) Palstra, T. T. M.; Steigerwald, M. L.; Ramirez, A. P.; Kwon, Y. U.; Stuczynski, S. M.; Schneemeyer, L. F.; Waszczak, J. V.; Zaanen, J. Electron correlations on a mesoscopic scale: Magnetic properties of transition metal telluride cluster compounds. *Phys. Rev. Lett.* **1993**, *71*, 1768−1771.

(19) Palstra, T. T. M.; Steigerwald, M. L.; Ramirez, A. P.; Zaanen, J. Electron correlations in transition metal-telluride cluster compounds. *Physica B: Condensed Matter* **1994**, *199*−*200*, 619−621.
(20) Nomikou, Z.; Schubert, B.; Hoffmann, R.; Steigerwald, M. L. Relationships between extended structures and molecular clusters of nickel and tellurium. *Inorg. Chem.* **1992**, *31*, 2201−2209.
(21) Lee, C.-H.; Liu, L.; Bejger, C.; Turkiewicz, A.; Goko, T.; Arguello, C. J.; Frandsen, B. A.; Cheung, S. C.; Medina, T.; Munsie, T. J. S.; D'Ortenzio, R.; Luke, G. M.; Besara, T.; Lalancette, R. A.; Siegrist, T.; Stephens, P. W.; Crowther, A. C.; Brus, L. E.; Matsuo, Y.; Nakamura, E.; Uemura, Y. J.; Kim, P.; Nuckolls, C.; Steigerwald, M. L.; Roy, X. Ferromagnetic Ordering in Superatomic Solids. *J. Am. Chem. Soc.* **2014**, *136*, 16926−16931.
(22) Fenske, D.; Krautscheid, H.; Müller, M. New Intermediate Steps in the Synthesis of Larger Nickel Clusters. *Angew. Chem., Int. Ed.* **1992**, *31*, 321−323.
(23) Data taken from a search of the *Cambridge Structural Database (CSD)*, Version 5.45, 2024 update. The search was restricted to homometallic APNCs.
(24) Touchton, A. J.; Wu, G.; Hayton, T. W. Generation of a Ni_3 Phosphinidene Cluster from the Ni(0) Synthon, $Ni(\eta^3\text{-}CPh_3)_2$. *Organometallics* **2020**, *39*, 1360−1365.
(25) Kagalwala, H. N.; Gottlieb, E.; Li, G.; Li, T.; Jin, R.; Bernhard, S. Photocatalytic Hydrogen Generation System Using a Nickel-Thiolate Hexameric Cluster. *Inorg. Chem.* **2013**, *52*, 9094−9101.
(26) Touchton, A. J.; Wu, G.; Hayton, T. W. Understanding the Early Stages of Nickel Sulfide Nanocluster Growth: Isolation of Ni_3, Ni_4, Ni_5, and Ni_8 Intermediates. *Small* **2021**, *17*, 2003133.
(27) Cook, A. W.; Hayton, T. W. Case Studies in Nanocluster Synthesis and Characterization: Challenges and Opportunities. *Acc. Chem. Res.* **2018**, *51*, 2456−2464.
(28) Cook, A. W.; Wu, G.; Hayton, T. W. A Re-examination of the Synthesis of Monolayer-Protected $Co_x(SCH_2CH_2Ph)_m$ Nanoclusters: Unexpected Formation of a Thiolate-Protected Co(II) T3 Super-tetrahedron. *Inorg. Chem.* **2018**, *57*, 8189−8194.
(29) Hosier, C. A.; Ackerson, C. J. Regiochemistry of Thiolate for Selenolate Ligand Exchange on Gold Clusters. *J. Am. Chem. Soc.* **2019**, *141*, 309−314.
(30) Li, S.; Li, N.-N.; Dong, X.-Y.; Zang, S.-Q.; Mak, T. C. W. Chemical Flexibility of Atomically Precise Metal Clusters. *Chem. Rev.* **2024**, *124*, 7262−7378.
(31) Hossain, S.; Kurashige, W.; Wakayama, S.; Kumar, B.; Nair, L. V.; Niihori, Y.; Negishi, Y. Ligand Exchange Reactions in Thiolate-Protected Au_{25} Nanoclusters with Selenolates or Tellurolates: Preferential Exchange Sites and Effects on Electronic Structure. *J. Phys. Chem. C* **2016**, *120*, 25861−25869.
(32) Gao, Z.-H.; Dong, J.; Zhang, Q.-F.; Wang, L.-S. Halogen effects on the electronic and optical properties of Au_{13} nanoclusters. *Nanoscale Adv.* **2020**, *2*, 4902−4907.
(33) Bai, M.; Qin, L.; Zeng, X.-M.; Wu, M.; Yao, L.-Y.; Yang, G.-Y. Dithiocarbonate-Protected Au_{25} Nanorods of a Chiral D_5 Configuration and NIR-II Phosphorescence. *J. Am. Chem. Soc.* **2024**, *146*, 12734−12742.
(34) Wang, Y.; Bürgi, T. Ligand exchange reactions on thiolate-protected gold nanoclusters. *Nanoscale Adv.* **2021**, *3*, 2710−2727.
(35) Hirai, H.; Takano, S.; Masuda, S.; Tsukuda, T. Introducing Iodide Ligands on $IrAu_{12}$ Cluster Enhances Phosphorescence Efficiency and Photoredox Activity. *ChemElectroChem* **2024**, *11*, No. e202300669.
(36) Yao, L.-Y.; Yam, V. W.-W. Diphosphine-Stabilized Small Gold Nanoclusters: From Crystal Structure Determination to Ligation-Driven Symmetry Breaking and Anion Exchange Properties. *J. Am. Chem. Soc.* **2016**, *138*, 15736−15742.
(37) Kang, X.; Zhu, M. Transformation of Atomically Precise Nanoclusters by Ligand-Exchange. *Chem. Mater.* **2019**, *31*, 9939−9969.
(38) Zeng, C.; Chen, Y.; Das, A.; Jin, R. Transformation Chemistry of Gold Nanoclusters: From One Stable Size to Another. *J. Phys. Chem. Lett.* **2015**, *6*, 2976−2986.
(39) Gao, Y.-Q.; Wu, W.-H.; Mao, H.; Zhang, Y.-G.; Zhan, C.-H.; Jiang, Z.-G. Transformations of silver(i) chalcogenide clusters induced by halide ions as dopant components rather than surface active species. *CrystEngComm* **2023**, *25*, 4934−4938.
(40) Du, W.; Deng, S.; Chen, S.; Jin, S.; Zhen, Y.; Pei, Y.; Zhu, M. Anisotropic Evolution of Nanoclusters from Ag_{40} to Ag_{45}: Halogen- and Defect-Induced Epitaxial Growth in Nanoclusters. *J. Phys. Chem. Lett.* **2021**, *12*, 6654−6660.
(41) Zou, X.; Kang, X.; Zhu, M. Recent developments in the investigation of driving forces for transforming coinage metal nanoclusters. *Chem. Soc. Rev.* **2023**, *52*, 5892−5967.
(42) Cui, M.; Shi, Y.; Ma, X.; Li, Q.; Chen, L.; Zhang, L.; Wu, J.; Yu, H.; Zhu, M. The Pivotal Radical Intermediate $[Au_{21}(SR)_{15}]^+$ in the Ligand-Exchange-Induced Size-Reduction of $[Au_{23}(SR)_{16}]^-$ to $Au_{16}(SR)_{12}$. *ACS Nano* **2024**, *18*, 6591−6599.
(43) Nguyen, T.-A. D.; Jones, Z. R.; Leto, D. F.; Wu, G.; Scott, S. L.; Hayton, T. W. Ligand-Exchange-Induced Growth of an Atomically Precise Cu_{29} Nanocluster from a Smaller Cluster. *Chem. Mater.* **2016**, *28*, 8385−8390.
(44) Wu, W.-H.; Zeng, H.-M.; Yu, Z.-N.; Wang, C.; Jiang, Z.-G.; Zhan, C.-H. Unusual structural transformation and luminescence response of magic-size silver(i) chalcogenide clusters via ligand-exchange. *Chem. Commun.* **2021**, *57*, 13337−13340.
(45) Smiles, D. E.; Wu, G.; Kaltsoyannis, N.; Hayton, T. W. Thorium−ligand multiple bonds via reductive deprotection of a trityl group. *Chem. Sci.* **2015**, *6*, 3891−3899.
(46) Williams, U. J.; Carroll, P. J.; Schelter, E. J. Synthesis and Analysis of a Family of Cerium(IV) Halide and Pseudohalide Compounds. *Inorg. Chem.* **2014**, *53*, 6338−6345.
(47) Touchton, A. J.; Wu, G.; Hayton, T. W. $[Ni_8(CN^tBu)_{12}][Cl]$: A nickel isocyanide nanocluster with a folded nanosheet structure. *J. Chem. Phys.* **2021**, *154*, 211102.
(48) Gonzàlez-Rosell, A.; Malola, S.; Guha, R.; Arevalos, N. R.; Matus, M. F.; Goulet, M. E.; Haapaniemi, E.; Katz, B. B.; Vosch, T.; Kondo, J.; Häkkinen, H.; Copp, S. M. Chloride Ligands on DNA-Stabilized Silver Nanoclusters. *J. Am. Chem. Soc.* **2023**, *145*, 10721−10729.
(49) Kulkarni, V. K.; Khiarak, B. N.; Takano, S.; Malola, S.; Albright, E. L.; Levchenko, T. I.; Aloisio, M. D.; Dinh, C.-T.; Tsukuda, T.; Häkkinen, H.; Crudden, C. M. *N*-Heterocyclic Carbene-Stabilized Hydrido Au_{24} Nanoclusters: Synthesis, Structure, and Electrocatalytic Reduction of CO_2. *J. Am. Chem. Soc.* **2022**, *144*, 9000−9006.
(50) Jin, R. Atomically precise metal nanoclusters: stable sizes and optical properties. *Nanoscale* **2015**, *7*, 1549−1565.
(51) Lummis, P. A.; Osten, K. M.; Levchenko, T. I.; Sabooni Asre Hazer, M.; Malola, S.; Owens-Baird, B.; Veinot, A. J.; Albright, E. L.; Schatte, G.; Takano, S.; Kovnir, K.; Stamplecoskie, K. G.; Tsukuda, T.; Häkkinen, H.; Nambo, M.; Crudden, C. M. NHC-Stabilized Au_{10} Nanoclusters and Their Conversion to Au_{25} Nanoclusters. *JACS Au* **2022**, *2*, 875−885.
(52) Narasimhan, L. R.; Palstra, T. T. M.; Tanzler, S. M.; Steigerwald, M. L. Relation between magnetic and structural anisotropy in the $Ni_{23}Se_{12}(PEt_3)_{13}$ cluster compound. *Phys. Rev. B* **1995**, *51*, 9337−9340.
(53) Shannon, R. D. Revised effective ionic radii and systematic studies of interatomic distances in halides and chalcogenides. *Acta Crystallogr., Sect. A* **1976**, *32*, 751−767.
(54) Evans, C. M.; Evans, M. E.; Krauss, T. D. Mysteries of TOPSe Revealed: Insights into Quantum Dot Nucleation. *J. Am. Chem. Soc.* **2010**, *132*, 10973−10975.
(55) Dean, P. A. W. Nuclear magnetic resonance studies of the solvation of phosphorus(V) selenides, 1,2-bis(diphenylphosphino)-ethane, and tris(dimethylamino)phosphine telluride by sulfur dioxide. *Can. J. Chem.* **1979**, *57*, 754−761.
(56) Jensen, K. A. Zur Stereochemie des koordinativ vierwertigen Nickels. *Z. anorg. allg. Chem.* **1936**, *229*, 265−281.
(57) Vihervaara, A.; Hatanpää, T.; Mizohata, K.; Chundak, M.; Popov, G.; Ritala, M. A low-temperature thermal ALD process for nickel utilizing dichlorobis(triethylphosphine)nickel(ii) and 1,4-bis-

https://doi.org/10.1021/acs.inorgchem.4c05088
Inorg. Chem. 2025, 64, 2926−2935

(trimethylgermyl)-1,4-dihydropyrazine. *Dalton Trans.* **2022**, *51*, 10898−10908.

https://doi.org/10.1021/acs.inorgchem.4c05088
Inorg. Chem. 2025, 64, 2926−2935